AIP | Journal of Applied Physics

Size and alloying induced shift in core and valence bands of Pd-Ag and Pd-Cu nanoparticles

Saurabh K. Sengar, B. R. Mehta, and Govind

Citation: Journal of Applied Physics **115**, 124301 (2014); doi: 10.1063/1.4869437
View online: http://dx.doi.org/10.1063/1.4869437
View Table of Contents: http://scitation.aip.org/content/aip/journal/jap/115/12?ver=pdfcov
Published by the AIP Publishing

Size and alloying induced shift in core and valence bands of Pd-Ag and Pd-Cu nanoparticles

Saurabh K. Sengar,[1] B. R. Mehta,[1,a)] and Govind[2]
[1]Thin Film Laboratory, Department of Physics, Indian Institute of Technology Delhi, New Delhi 110016, India
[2]Surface Physics Group, National Physical Laboratory (CSIR), New Delhi 110012, India

(Received 6 March 2014; accepted 13 March 2014; published online 25 March 2014)

In this report, X-ray photoelectron spectroscopy studies have been carried out on Pd, Ag, Cu, Pd-Ag, and Pd-Cu nanoparticles having identical sizes corresponding to mobility equivalent diameters of 60, 40, and 20 nm. The nanoparticles were prepared by the gas phase synthesis method. The effect of size on valence and core levels in metal and alloy nanoparticles has been studied by comparing the values to those with the 60 nm nanoparticles. The effect of alloying has been investigated by comparing the valence and core level binding energies of Pd-Cu and Pd-Ag alloy nanoparticles with the corresponding values for Pd, Ag, and Cu nanoparticles of identical sizes. These effects have been explained in terms of size induced lattice contractions, alloying induced charge transfer, and hybridization effects. The observation of alloying and size induced binding energy shifts in bimetallic nanoparticles is important from the point of view of hydrogen reactivity.
 [http://dx.doi.org/10.1063/1.4869437]

I. INTRODUCTION

Palladium is an important material in hydrogen gas sensing, hydrogen production membranes, and hydrogen storage applications because of its selectivity, low activation energy, large sticking and diffusion coefficients, and sensitivity towards hydrogen.[1–3] The alloying of Pd with other metals changes its structural and electronic properties, which can have significant effect on Pd-H interaction.[4] The ordered Pd-Cu (bulk) structure is reported to have high selectivity towards hydrogenation of ethylene in comparison with the disordered Pd-Cu structure.[5,6] The binary Pd-M (M = Cu and Fe) systems have been identified as promising polymer electrolyte fuel cell (PEFC) cathode electrocatalysts, with enhanced activity for oxygen reduction reaction (ORR) and stability as compared to Pd alone.[7,8] The origin of the enhanced activity has been linked to modification of the electronic structure of Pd upon bonding with the alloying metal.[9] In addition to alloying, the structural and electronic properties of the Pd can also be tailored by reducing its dimensions. The Pd nanoparticles have shown better hydrogenation properties in comparison to their thin film and bulk counterparts.[10–14] The increased surface area and quantum confinement effects in the nanoparticles alter their electronic properties, resulting in enhanced activity and specificity of the catalysts.[15] The effect of alloying and size on the electronic properties of Pd can be clearly understood by synthesizing Pd-alloy nanoparticles with controlled dimensions. In earlier reports, there have been some efforts towards synergizing the useful effects of alloying and size reduction by preparing Pd-alloy nanoparticles.[16–21] The electronic properties of Pd-Ag and Pd-Cu alloy nanoparticles have been studied as a function of composition using the chemical synthesis routes.[16,17,20,21] Sequential or co-evaporation of the two components using e-beam, thermal heating, sputtering, and laser ablation has been used to prepare Pd-Cu and Pd-Ag alloy thin films and nanoparticulate layers having large variations in composition or phase impurity. Furthermore, size and density of the clusters are controlled by the deposition time. In the above methods, substrate effects results in growth of two dimensional alloy nanostructures or discontinuous films.[22] The lack of size and composition control, which is a stringent requirement for a clear understanding of size and alloying effects, is the major nagging issue in the above studies. Gas phase growth technique used in the present study overcomes the above mentioned limitation as the 3D spherical particle growth occurs in a homogeneous gaseous medium and well formed spherical nanoparticles are deposited on substrates in the final step thus avoiding any substrate effects.

In the present study, electronic properties of Pd–Cu and Pd-Ag alloy nanoparticles having well-defined sizes (D_m = 20, 40, and 60 nm), narrow size distribution, and a constant composition have been studied. It is important to note that the effect of nanoparticle size on electronic properties has been studied by comparing the binding energy values with those of the corresponding 60 nm size nanoparticles, on the other hand, the effect of alloying has been understood by comparing the binding energy values of Pd-Ag, Pd-Cu alloy nanoparticles with those of the Pd, Ag, and Cu nanoparticles of identical sizes.

II. EXPERIMENT

An integrated gas phase synthesis set up was used for the synthesis of Pd, Cu, Ag, Pd-Ag, and Pd-Cu nanoparticles.[23,24] The setup consists of a spark generator, a neutralizer, a differential mobility analyser (DMA), a sintering furnace, and an electrostatic precipitator (ESP). The spark generator is used to produce initial primary nanoparticles which are converted into loosely connected agglomerate

a)Author to whom correspondence should be addressed. Electronic mail: brmehta@physics.iitd.ac.in

structures due to the collisions with each other during their journey to neutralizer. Neutralizer is a general term used to describe the equipment for obtaining a known charge distribution of aerosol particles. After charging, the agglomerates are selected according to their electrical mobility using the DMA. In aerosol technology, DMA is frequently used to select the particles of certain mobility by varying the applied voltage and sheath flow conditions. After size selection, agglomerates are sintered in a horizontal tubular furnace where they undergo compaction, and finally, monodisperse, crystalline and spherical nanoparticles are formed at appropriate temperatures. The positioning of the sintering furnace after size selection step allows the optimization of sintering temperature for nanoparticles of different sizes. In ESP, nanoparticles are directed towards the desired substrates and transmission electron microscopy (TEM) grids, kept perpendicular at a distance of 1.5 mm from the nozzle for the final deposition. The detailed description of the gas phase synthesis setup can be seen elsewhere.[23,24]

For the synthesis of Pd, Ag, and Cu nanoparticles, commercially available aerosol generator (GFG 1000, Palas, Gmbh, Germany) was modified by replacing both the graphite rods by Pd, Ag, and Cu rods, respectively. The Cu and Pd rods were used for the synthesis of Pd-Cu nanoparticles, while Ag and Pd rods were used for the synthesis of Pd-Ag alloy nanoparticles. Each of the metal rods (Pd, Ag and Cu) has a diameter of 3.2 mm. The distance between the two electrodes (rods) is kept fixed at 1.8 mm using a stepper motor. The spark frequency was kept fixed at 200 Hz, while a constant flow (2.8 l/min) of nitrogen carrier gas was maintained during the synthesis of the nanoparticles. After spark generator, the carrier gas flow was reduced to 1.0 l/min during particle charging in neutralizer, size selection in DMA, in-flight sintering in the furnace, and deposition in ESP. The DMA is mainly made up of two concentric metal cylinders, the inner solid cylinder and the outer hollow cylinder. Outer cylinder is kept at zero potential, while inner cylinder is kept a negative potential by connecting it to a high voltage supply. Three different size selected Pd, Ag, Cu, Pd-Cu, and Pd-Ag agglomerates having mobility equivalent diameter (D_m) values of 20, 40, and 60 nm were selected by applying the voltage of 0.670, 2.564, 5.498 kV, respectively, on the inner electrode of DMA, The ratio of carrier to sheath gas flow in DMA was fixed at 1:10. In the sintering furnace, the temperature was optimized for all the three sizes of Pd, Ag, Cu, Pd-Ag, and Pd-Cu to compact them into crystalline and spherical nanoparticles. The residence time of the nanoparticles in the sintering furnace is 18 s. It must be mentioned that over-sintering leads to re-evaporation of the nanoparticles, while under-sintering leads to non-spherical shape. The Pd and Pd-Ag nanoparticles having D_m values of 20, 40, and 60 nm were sintered at 500, 700, and 900 °C, respectively, while the Pd-Cu nanoparticles were sintered at a little higher temperature of 520, 720, and 920 °C, respectively. The optimized sintering temperature for Cu nanoparticles was found to be 410, 540, and 690 °C, respectively. The Ag nanoparticles were sintered at a relatively lower temperature of 260 °C, 340 °C, and 440 °C, respectively. Finally, in the ESP, a constant voltage of 1 KeV was applied to the substrate to deposit the sintered nanoparticles.

TEM analysis of the deposited Pd, Ag, Cu, Pd-Ag, and Pd-Cu alloy nanoparticles was done to study the size and structural properties using FEI-Technai-G20 with a LaB6 filament (operated at 200 kV). Glancing angle x-ray diffraction (GAXRD) measurements at a glancing angle of 2° were carried out to investigate the structural properties using Philips X'Pert, PRO-PW 3040. X-ray photoelectron microscopy (XPS) measurements were performed using Model 1257, Perkin Elmer, USA equipment. Valence and core level spectra of the samples were obtained using Al K_α radiation as the excitation source after 10 min Ar ion cleaning. The binding energy values were referenced using the C 1 *s* peak position at 284.6 eV.

III. RESULTS AND DISCUSSION

In the present study, XPS investigations have been carried out on Pd-Ag and Pd-Cu nanoparticles having D_m values of 20, 40, and 60 nm and compared with those of Pd, Ag, and Cu nanoparticles prepared under identical conditions and having similar D_m values. The TEM micrographs of sintered Pd, Pd-Ag, and Pd-Cu nanoparticles having the initial D_m value of 20 nm are shown in Fig. 1. It is clear from the micrographs that nanoparticles are nearly spherical and monodisperse. The average size (D_g) of the Pd, Pd-Ag, and Pd-Cu nanoparticles after complete compaction and crystallization on sintering is observed to be 8.9, 9.7, and 10.3 nm with a standard deviation of 0.53, 0.61, and 0.83, respectively. Furthermore, nanoparticles obtained after sintering are nearly spherical and monocrystalline in nature as is clear from the HRTEM micrograph of a sintered Pd nanoparticle (Fig. 1(d)). The detailed characterizations of the nanoparticles in terms of size, structure, and composition have been carried out and the results are explained elsewhere.[4,24] The

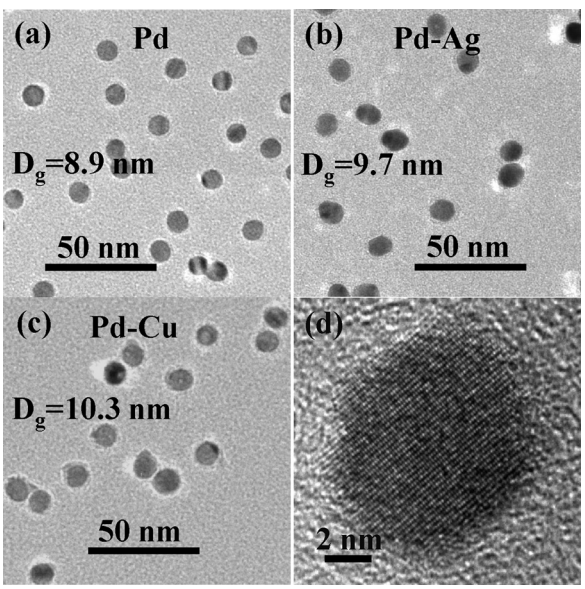

FIG. 1. TEM micrographs of sintered (a) Pd, (b) Pd-Ag, and (c) Pd-Cu nanoparticles having an initial D_m value of 20 nm. HRTEM micrograph (d) of a sintered Pd nanoparticle (Dg = 9 nm) is also shown.

(111) XRD peak positions of Pd, Ag, Cu, Pd-Ag, and Pd-Cu nanoparticles were observed to shift towards higher 2θ values (lower d-values), indicating a lattice contraction of 0.23, 0.29, 0.25, 0.20, and 0.26%, respectively, on decreasing the size (D_m) from 60 nm to 20 nm. The observed lattice contraction in the nanoparticles can be attributed to the enhanced surface area and surface bond contraction with coordination number reduction at lower particle size. The lattice contraction in Au, Sn, Ni, and Bi nanoparticles has been reported on decreasing the particle size.[25–28] Energy dispersive x-ray analysis (EDAX) was used to obtain the composition of Pd-Ag and Pd-Cu nanoparticles having D_m values of 20, 40, and 60 nm. The Pd/M (M = Ag and Cu) atomic ratio is found to be fixed at 55:45 and 68:32 in Pd-Ag and Pd-Cu nanoparticles, respectively, for all the three sizes ($D_m = 20$, 40, and 60 nm).

In this study, the effect of nanoparticle size has been determined by comparing the XPS peak positions of Pd, Cu, Ag, Pd-Ag, and Pd-Cu nanoparticles of different sizes with those of the nanoparticles of 60 nm size. Similarly, effect of alloying has been determined by comparing the binding energy values of Pd-Ag and Pd-Cu alloy nanoparticles having D_m values of 60, 40, and 20 nm with those of Pd, Ag, or Cu metal nanoparticles of identical sizes. The XPS core level binding energy spectra of Pd, Ag, and Cu nanoparticles having D_m values of 60 nm are shown in Figs. 2(a)–2(c). In case of Pd, Ag, and Cu nanoparticles, Pd3d5/2, Ag3d5/2, and Cu2p3/2 core level binding energy peaks lie at 335.35 eV, 367.90 eV, and 931.36 eV, respectively. The above values match closely with the earlier reported bulk values.[29–31] It is observed that Pd 3d5/2, Ag 3d5/2, and Cu2p3/2 core level peaks are asymmetric towards the high binding energy side, which may be due to the adsorbed surface oxygen or large fraction of surface atoms in the nanoparticles. The above effects will result in the binding energy increase and hence a tail may appear on the high binding energy side. Pd3d5/2, Ag3d5/2, and Cu2p3/2 core level peak positions of Pd, Ag, and Cu nanoparticles having D_m values of 20 and 40 nm were also calculated from the XPS core level spectra. The shift in the binding energy value (ΔE_S) of Pd 3d5/2, Ag 3d5/2, and Cu 2p3/2 core levels on decreasing the size of Pd, Ag, and Cu nanoparticles is shown in Fig. 2(d). It is important to mention that ΔE_S is the shift in binding energy value of the nanoparticles on decreasing the size with respect to the corresponding binding energy of the 60 nm sized nanoparticles. It can be observed that at 40 nm size ΔE_S is very less and it increases on further decreasing the size of the nanoparticles to 20 nm, indicating an increase in binding energy on decreasing the nanoparticle size. In earlier reports, increase in binding energy on decreasing the crystallite size of Ag, Cu, and Sn crystallites in vacuum evaporated thin films has been reported.[32–34] The XRD results reported elsewhere show that increase in binding energy on decreasing the particle size may be attributed to decreased lattice parameter.[31] It has been shown that lattice distortion alters the chemical bonding, which in turn leads to changes in the core and valence band binding energies.[33] Mason *et al.* argued that changes in the electron configuration of the atoms in smaller clusters are primarily responsible for the shift.[35] Furthermore, shift in binding energy is related to the lattice strain that exists because the average bond distances in small clusters are shorter than in the bulk.[36,37] The chemical changes important for the binding energy shift involve an increased *d* to *sp* promotion (or hybridization) for shorter bond distances, resulting in the increased binding energy.[33] Smaller nanoparticles ($D_m = 20$ nm) have lower value of lattice constant with respect to their bulk counterparts, while values for larger size nanoparticles ($D_m = 60$ nm) approach

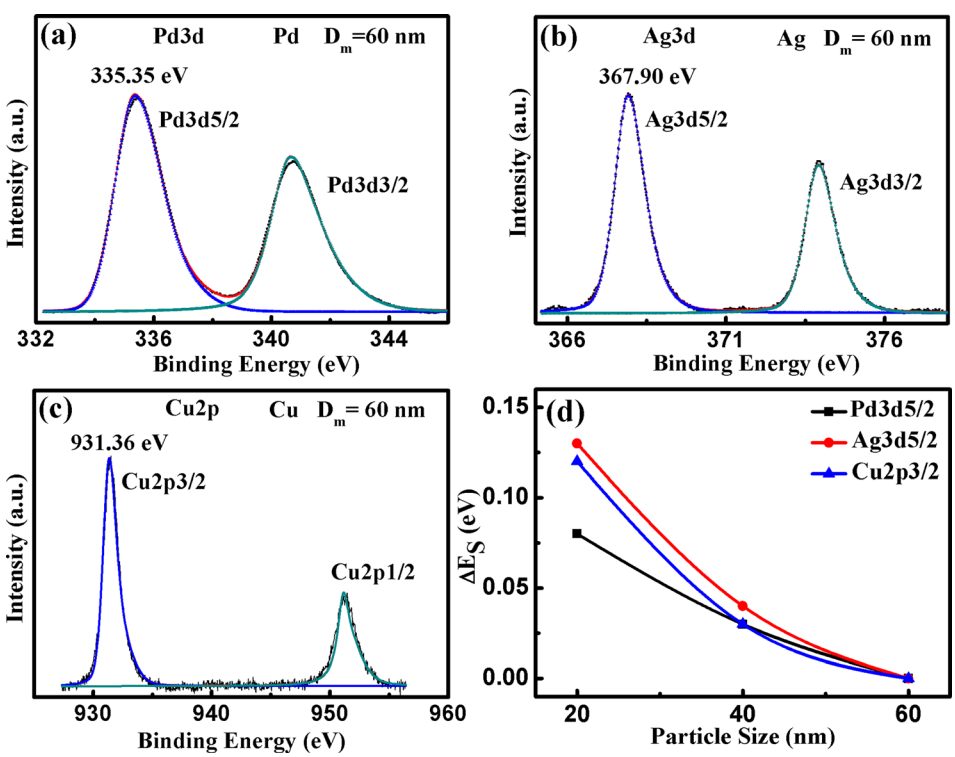

FIG. 2. XPS core level spectra of (a) Pd, (b) Ag, and (c) Cu nanoparticles ($D_m = 60$ nm). (d) Shift in binding energy (ΔE_S) as a function of the nanoparticle size.

the bulk value. Thus, the increase in binding energy on decreasing the size in Pd, Ag, and Cu nanoparticles is consistent with the observed lattice contraction.

The Pd4d, Ag4d, and Cu3d valence band spectra of Pd, Ag, and Cu nanoparticles having $D_m = 60$ nm are shown in Figs. 3(a)–3(c). It can be seen that Pd4d extends from nearly −2 to 10 eV, Ag4d extends from 0 to 10 eV and Cu3d extends from 0 to 5 eV. The centroid of Pd4d, Ag4d, and Cu3d lies at 2.39, 4.78, and 2.28 eV, respectively, which are close to the reported bulk values.[32,38,39] In addition, centroid positions of valence band spectra of Pd, Ag and Cu nanoparticles having $D_m = 20$ and 40 nm were also calculated. The change in centroid position (ΔE_S) in Pd4d, Ag4d, and Cu3d on decreasing the size is shown graphically in Fig. 3(d). It can be seen that in 40 nm particles ΔE_S is appreciable, especially in Cu ($\Delta E_S = 0.1$ eV). On further decreasing the particle size to 20 nm, ΔE_S increases, indicating that valence band centroid shifts away from the Fermi energy. It may be noted that although the trend of valence band shift is similar to that observed in core levels but the magnitude is relatively large. This indicates that in metals, lattice distortion effects are dominant in valence band binding energy values in comparison with the core level binding energy values. Valence bands take part in bonding and any effect on bond length, disorder, or coordination number influence valence band binding energy more in comparison to core levels.

The Pd3d5/2, Cu2p3/2, and Ag3d5/2 core level spectra corresponding to 60 nm sized Pd-Ag and Pd-Cu alloy nanoparticles are shown in Fig. 4. It is observed that Pd3d5/2 and Cu2p3/2 core level peaks in Pd-Cu nanoparticles lie at 335.15 and 931.53 eV, respectively. The Pd3d5/2 and Cu2p3/2 core level peak positions in Pd-Cu alloy nanoparticles are shifted by −0.20 eV and 0.17 eV in comparison with the corresponding bulk values of Pd and Cu metals, which may be attributed to the alloy formation. The observed –ve shift in Pd3d5/2 and +ve shift in Cu2p3/2 indicate charge transfer from Cu to Pd. Because of the charge transfer resulting from the electronegativity differences, binding energy values of the constituent elements shift in the opposite direction. Pd is more electronegative (2.2) than Cu (1.9), which results in the charge flow from Cu to Pd on alloying, and hence, the binding energy of Pd decreases while that of Cu increases. In case of Pd-Ag nanoparticles having $D_m = 60$ nm, Pd3d5/2 and Ag3d5/2 core level peaks in Pd-Ag nanoparticles lie at 335.25 and 367.34 eV, respectively. These values exhibit a shift of −0.1 eV and −0.56 eV with respect to the corresponding Pd and Ag bulk values. In the context of the simple electronegativity picture, charge transfer would be expected from Ag to Pd upon alloying, since Pd is more electronegative than Ag. Although this argument works well for compounds of non-transition elements, it is generally not valid for metallic alloys with full or nearly full d-bands.[40,41] In particular, it is observed that the 3d core level shifts of both Ag and Pd have the same sign.[42] Abrikosov *et al.* have explained this behaviour in terms of *intra*-atomic charge re-distribution due to valence electron hybridization.[42] Thus, the observed –ve shifts of 0.1 eV and 0.56 eV in Pd3d5/2 and Ag3d5/2 with respect to the corresponding Pd and Ag bulk values indicate the alloy formation in Pd-Ag nanoparticles having $D_m = 60$ nm. The shift in the binding energy value (ΔE_S) of Pd 3d5/2, Ag 3d5/2, and Cu 2p3/2 core levels on decreasing the size of Pd-Ag and Pd-Cu nanoparticles as a function of size is shown in Figs. 5(a) and

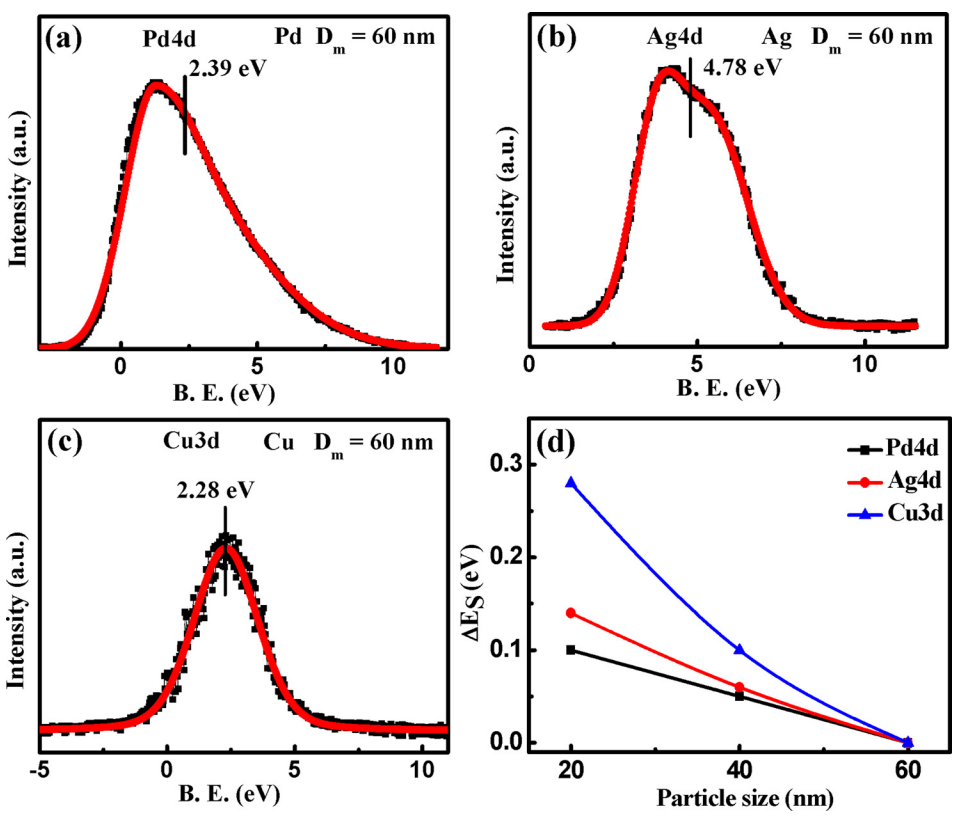

FIG. 3. XPS valence band spectra of (a) Pd, (b) Ag, and (c) Cu nanoparticles ($D_m = 60$ nm). (d) Shift in binding energy (ΔE_S) is shown as a function of nanoparticle size.

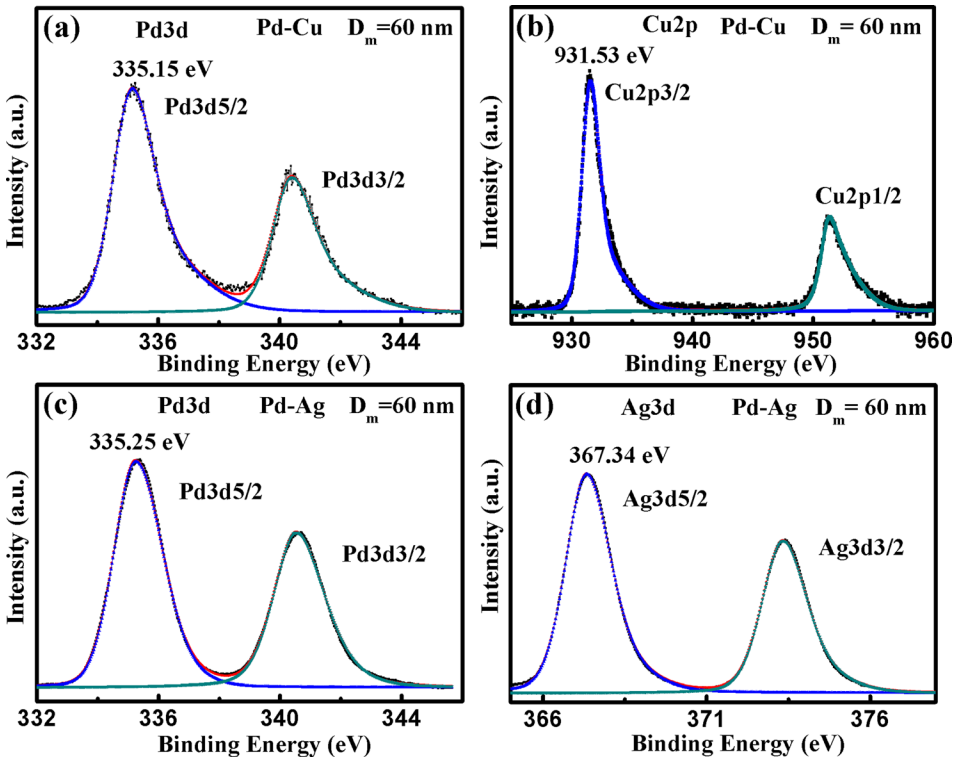

FIG. 4. XPS core level spectra of (a) and (b) Pd-Cu and (c) and (d) Pd-Ag alloy nanoparticles ($D_m = 60$ nm).

5(b). It is evident that as we decrease the size of the Pd-Cu and Pd-Ag alloy nanoparticles, ΔE_S increases which means that binding energy increases. Since the composition is similar for all the particle sizes in both the Pd-Cu and Pd-Ag nanoparticles, the increase in binding energy may be attributed to the decrease in lattice parameter. Earlier also shift in core level binding energies on decreasing the cluster size is reported in Pd-Cu and Pd-Ni clusters prepared by the physical evaporation techniques.[43,44] It must be noted that the values of ΔE_S increase faster in Pd-alloy nanoparticles in comparison to Pd, Ag, and Cu metal nanoparticles. This indicates that size induced effects leading to bond length contraction which result in redistribution/hybridization of valence charges, are dominant in alloys in comparison to metal nanoparticles.

The valence band spectra of Pd-Ag and Pd-Cu alloy nanoparticles having $D_m = 60$ nm are shown in Figs. 6(a) and 6(b). It is evident that the valence band spectrum of Pd-Ag extends from −2 to 10 eV while that of Pd-Cu extends from −1 to 9 eV. In Pd-Ag alloy nanoparticles, valence band has two contributions corresponding to Pd4d and Ag4d, as shown in Fig. 6(a). Similarly, in Pd-Cu alloy nanoparticles, valence band has two contributions corresponding to Pd4d and Cu3d. The centroids of the Pd4d and Ag4d in Pd-Ag nanoparticles lie at 2.11 eV and 4.82 eV while those of Pd4d and Cu3d in Pd-Cu nanoparticles lie at 1.99 eV and 2.54 eV, respectively. Furthermore, the centroid positions of the Pd4d and Ag4d valence contributions in Pd-Ag nanoparticles and Pd4d and Cu3d valence contribution in Pd-Cu nanoparticles having $D_m = 20$ and 40 nm were also calculated. The shift in valence band binding energy (ΔE_S) on decreasing the size of Pd-Ag and Pd-Cu nanoparticles is shown in Figs. 6(c) and 6(d). It is observed that ΔE_S increases on decreasing the size. This trend of increase in ΔE_S in the valence bands of Pd-Ag and Pd-Cu is similar to that observed in core levels but is larger in magnitude. The above again confirms that lattice distortion influences valence band binding energy values more in comparison with core level binding energy values.

By comparing the binding energy values in Pd-Ag and Pd-Cu nanoparticles with those of the Pd, Ag, and Cu nanoparticles having similar sizes, the effect of alloying (ΔE_a) on

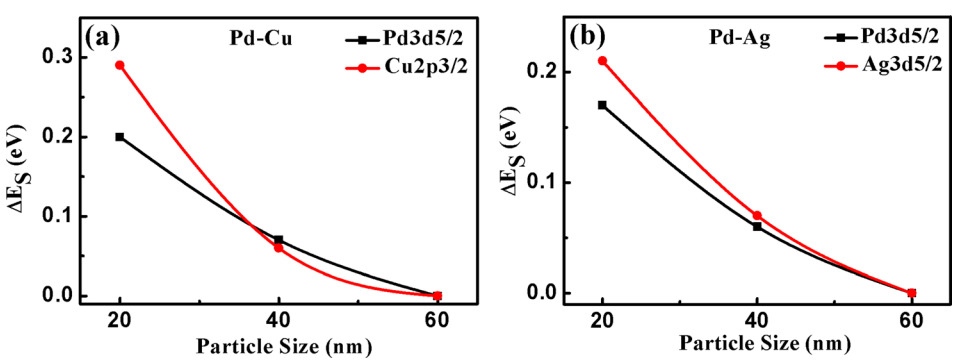

FIG. 5. Shift in binding energy (ΔE_S) as a function of nanoparticle size in (a) Pd-Cu and (b) Pd-Ag alloy nanoparticles.

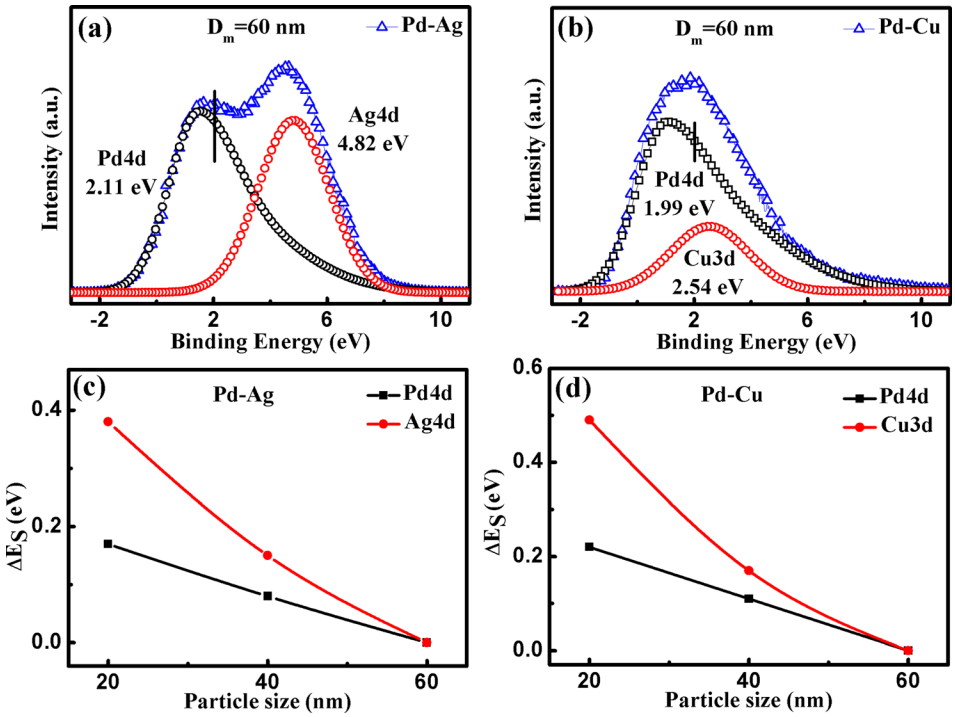

FIG. 6. XPS valence band spectra of (a) Pd-Ag and (b) Pd-Cu alloy nanoparticles ($D_m = 60$ nm). The shift in binding energy (ΔE_S) as a function of nanoparticle size in (c) Pd-Ag and (d) Pd-Cu alloy nanoparticles.

core level and valence band binding energy values has been determined. It may be noted that ΔE_a is the shift in core level/valence band peak position in Pd-Cu and Pd-Ag nanoparticles with respect to the corresponding position in Pd, Cu, and Ag nanoparticles having similar size. Fig. 7 exhibits the variation in ΔE_a as a function of size. In Pd-Cu nanoparticles, ΔE_a is –ve for Pd3d5/2 and +ve for Cu2p3/2. It is also observed that the ΔE_a decreases (in magnitude) for Pd3d5/2 and increases for Cu2p3/2 on decreasing the size (Fig. 7(a)). Similar behaviour in valence bands of Pd-Cu nanoparticles is also observed (Fig. 7(b)). ΔE_a for Pd4d is –ve and decreases (in magnitude) while for Cu3d, ΔE_a is +ve and increases on decreasing the size (Fig. 7(b)). Furthermore, the magnitude of ΔE_a for valence levels is larger in comparison with core levels. The alloying induced binding energy shift (ΔE_a) in core level and valence band of Pd-Cu nanoparticles can be explained on the basis of charge transfer on alloying due to electronegativity differences. Since the core levels are relatively compact and are generally assumed not to take part in the bonding, charge transfer is expected to affect valence level electrons more in comparison with core levels, and hence, ΔE_a for valence levels is in general more than that of

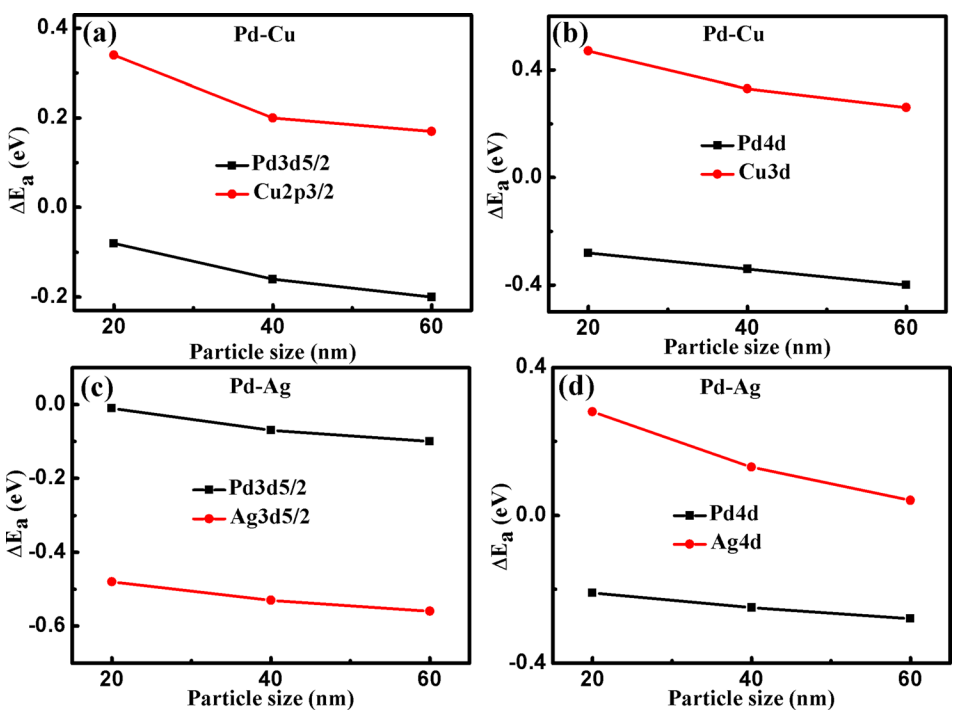

FIG. 7. Shift in binding energy (ΔE_a) on alloying as a function of size in core levels [(a) and (c)] and valence bands [(b) and (d)] in Pd-Cu and Pd-Ag alloy nanoparticles.

core levels. Similar trend of core level shift in Pd-Cu nanoparticles (increase in the magnitude of ΔE_a on decreasing the particle size) is reported on decreasing the Pd concentration in Pd-Cu bulk alloys.[45] In Pd-Ag nanoparticles, ΔE_a for both the Pd3d5/2 and Ag3d5/2 is –ve and their magnitude decreases with reduction in nanoparticle size (Fig. 7(c)). In contrast to core levels, ΔE_a is –ve for Pd4d and +ve for Ag4d valence bands and decreases (in magnitude) for Pd4d while increases in Ag4d on decreasing the size (Fig. 7(d)). The sign and magnitude of ΔE_a in Pd4d and Ag4d indicate that it is due to electron transfer but ΔE_a in Pd3d5/2 and Ag3d5/2 has the same –ve sign which cannot be explained on the basis of electron transfer. The –ve value of ΔE_a in both the Pd3d5/2 and Ag3d5/2 has been explained by Abrikosov *et al*. on the basis of charge re-distribution due to alloying.[42] Furthermore, a similar increasing trend of core and valence level shifts (increase in the magnitude of ΔE_a on decreasing the particle size) is reported in Pd-Ag bulk alloys on decreasing the Pd concentration.[42] In alloys, the change in binding energy (ΔE_a) is mainly because of interatomic charge transfer (due to electronegativity difference) and hybridization. In hybridization, intra-atomic charge re-distribution takes place. Both the change in composition and the decrease in particle size result in intra-atomic charge re-distribution or hybridization.[33,42] The effect of hybridization is reported to increase on decreasing the size in metals or changing the alloy composition.[33,42] In the present study, alloy composition is constant at all the particle sizes. The effect of hybridization has been removed by subtracting the metal binding energies of the same size metal nanoparticles. The observed increase in ΔE_a on decreasing the size of Pd-Ag and Pd-Cu nanoparticles indicates that the effect of hybridization is stronger in alloys in comparison to metals at lower sizes.

IV. CONCLUSIONS

The size selected metal and alloy nanoparticles having D_m values of 20, 40 and 60 nm were successfully prepared by the gas phase deposition method and their XPS studies were carried out. The binding energy values in Pd, Ag, and Cu metal nanoparticles show an increase in magnitude due to size induced lattice contraction. Increase in binding energy is larger in valence band in comparison with core levels. Similar trend of increase in binding energy value on decreasing the size is observed in Pd-Ag and Pd-Cu alloy nanoparticles; but the magnitude is larger in comparison with metal nanoparticles. In case of Pd-Cu nanoparticles, opposite sign of binding energy shift for Pd and Cu peaks is consistent with the charge transfer due to electronegativity difference. In case of Pd-Ag nanoparticles, alloying induced shift is due to the hybridization effects. It is also observed that hybridization effects are strong in alloy nanoparticles in comparison to metal nanoparticles at lower sizes.

ACKNOWLEDGMENTS

One of the authors, Saurabh K. Sengar is thankful to Council of Scientific and Industrial Research (CSIR), India for providing senior research fellowship. One of the authors (B.R.M.) gratefully acknowledges the support of Nanomission Programme of Department of Science and Technology (DST), India and Schlumberger Chair Professorship.

[1]B. Dean, A. A. Haasz, and P. C. Stangeby, J. Vac. Sci. Technol. A **5**, 2332 (1987).
[2]J.-S. Noh, J. M. Lee, and W. Lee, Sensors **11**, 825 (2011).
[3]D. B. Wolfe, J. C. Love, K. E. Paul, M. L. Chabinyc, and G. M. Whitesides, Appl. Phys. Lett. **80**, 2222 (2002).
[4]S. K. Sengar, B. R. Mehta, P. K. Kulriya, and S. A. Khan, Appl. Phys. Lett. **103**, 173107 (2013).
[5]M. Friedrich, S. Villaseca, L. Szentmiklósi, D. Teschner, and M. Armbrüster, Materials **6**, 2958 (2013).
[6]J. Völkl and G. Alefeld, *Diffusion of Hydrogen in Metals* (Springer Berlin Heidelberg, 1978), Vol. 28.
[7]M.-H. Shao, K. Sasaki, and R. R. Adzic, J. Am. Chem. Soc. **128**, 3526 (2006).
[8]C. Xu, Y. Zhang, L. Wang, L. Xu, X. Bian, H. Ma, and Y. Ding, Chem. Mater. **21**, 3110 (2009).
[9]M. Shao, P. Liu, J. Zhang, and R. Adzic, J. Phys. Chem. B **111**, 6772 (2007).
[10]A. Pundt, C. Sachs, M. Winter, M. T. Reetz, D. Fritsch, and R. Kirchheim, J. Alloys Compd. **293–295**, 480 (1999).
[11]A. Pundt and R. Kirchheim, *Hydrogen in Metals: Microstructural Aspects* (Annual Reviews, Palo Alto, 2006).
[12]M. Khanuja, B. R. Mehta, P. Agar, P. K. Kulriya, and D. K. Avasthi, J. Appl. Phys. **106**, 093515 (2009).
[13]M. Khanuja, D. Varandani, and B. R. Mehta, Appl. Phys. Lett. **91**, 253121 (2007).
[14]I. Aruna, B. R. Mehta, and L. K. Malhotra, Appl. Phys. Lett. **87**, 103101 (2005).
[15]J. S. Bradley, *Cluster and Colloids* (VCH, New York, 1994).
[16]A. M. Venezia, L. F. Liotta, G. Deganello, Z. Schay, and L. Guczi, J. Catal. **182**, 449 (1999).
[17]N. N. Kariuki, X. Wang, J. R. Mawdsley, M. S. Ferrandon, S. G. Niyogi, J. T. Vaughey, and D. J. Myers, Chem. Mater. **22**, 4144 (2010).
[18]H. Ye and R. M. Crooks, J. Am. Chem. Soc. **129**, 3627 (2007).
[19]D. Wang, A. Villa, F. Porta, L. Prati, and D. Su, J. Phys. Chem. C **112**, 8617 (2008).
[20]K. Torigoe and K. Esumi, Langmuir **9**, 1664 (1993).
[21]W. Wang and G. Cao, J. Nanopart. Res. **9**, 1153 (2007).
[22]H. Naganuma, K. Sato, and Y. Hirotsu, J. Appl. Phys. **100**, 074914 (2006).
[23]S. K. Sengar, B. R. Mehta, R. Kumar, and V. Singh, Sci. Rep. **3**, 2814 (2013).
[24]S. K. Sengar, B. R. Mehta, and Govind, J. Appl. Phys. **112**, 014307 (2012).
[25]I. Aruna, B. R. Mehta, L. K. Malhotra, and S. M. Shivaprasad, J. Appl. Phys. **104**, 064308 (2008).
[26]Q. S. Chang, J. Phys. Condens. Matter **11**, 4801 (1999).
[27]O. Cheshnovsky, K. J. Taylor, J. Conceicao, and R. E. Smalley, Phys. Rev. Lett. **64**, 1785 (1990).
[28]Z. M. Stadnik, P. Griesbach, G. Dehe, P. Gütlich, T. Kohara, and G. Stroink, Phy. Rev. B **35**, 6588 (1987).
[29]P. Légaré, F. Finck, R. Roche, and G. Maire, Surf. Sci. **217**, 167 (1989).
[30]J. C. Fuggle, E. Källne, L. M. Watson, and D. J. Fabian, Phy. Rev. B **16**, 750 (1977).
[31]S. K. Sengar, B. R. Mehta, and G. Gupta, Appl. Phys. Lett. **98**, 193115 (2011).
[32]G. K. Wertheim, S. B. DiCenzo, and D. N. E. Buchanan, Phy. Rev. B **33**, 5384 (1986).
[33]B. Richter, H. Kuhlenbeck, H. J. Freund, and P. S. Bagus, Phys. Rev. Lett. **93**, 026805 (2004).
[34]G. K. Wertheim and S. B. DiCenzo, Phy. Rev. B **37**, 844 (1988).
[35]M. G. Mason, Phy. Rev. B **27**, 748 (1983).
[36]S. A. Nepijko, M. Klimenkov, M. Adelt, H. Kuhlenbeck, R. Schlögl, and H. J. Freund, Langmuir **15**, 5309 (1999).
[37]M. Klimenkov, S. Nepijko, H. Kuhlenbeck, M. Bäumer, R. Schlögl, and H. J. Freund, Surf. Sci. **391**, 27 (1997).
[38]S. Chaturvedi, J. Rodriguez, T. Jirsak, and J. Hrbek, Surf. Sci. **412–413**, 273 (1998).

[39]G. Marek, E. Andreas, and H. Jürgen, J. Phys. Condens. Matter **16**, 1141 (2004).
[40]T. K. Sham, Phy. Rev. B **31**, 1888 (1985).
[41]I. Coulthard and T. K. Sham, Phys. Rev. Lett. **77**, 4824 (1996).
[42]I. A. Abrikosov, W. Olovsson, and B. Johansson, Phys. Rev. Lett. **87**, 176403 (2001).
[43]K. R. Harikumar, S. Ghosh, and C. N. R. Rao, J. Phys. Chem. A **101**, 536 (1997).
[44]A. K. Santra, G. N. Subbanna, and C. N. R. Rao, Surf. Sci. **317**, 259 (1994).
[45]W. Olovsson, I. A. Abrikosov, and B. Johansson, J. Electron. Spectrosc. Relat. Phenom. **127**, 65 (2002).